J Mater Sci (2008) 43:6960–6966
DOI 10.1007/s10853-008-2965-7

# Role of molybdenum on the AISI 316L oxidation at 900 °C

**H. Buscail · S. El Messki · F. Riffard · S. Perrier · R. Cueff · C. Issartel**

Received: 9 April 2008 / Accepted: 20 August 2008 / Published online: 17 September 2008
© Springer Science+Business Media, LLC 2008

**Abstract** In situ X-ray diffraction was used to study the oxide formation on AISI 316L stainless steel (SS) specimens during isothermal oxidation at 900 °C in air. Results were compared with those obtained on AISI 304 SS to determine the role of molybdenum on the oxidation process for the AISI 316L SS specimens. Our results show that molybdenum plays a major protective role during steel oxidation. This element is found in a $NiMoO_4$ phase at the internal oxide–metal interface. The high molybdenum content of the alloy hinders the outward diffusion of iron and leads to a lower growth rate and better scale adherence. The oxide scale is then composed of $Cr_2O_3$ with a small amount of $Mn_{1.5}Cr_{1.5}O_4$ at the external interface. The improved scale adherence appears to be due to a keying effect at the scale/alloy interface promoted by molybdenum.

## Introduction

Due to its good creep properties and the oxidation resistance provided by chromium, AISI 316L austenitic stainless steel (SS) is a technologically important SS widely used in industrial applications [1–6]. However, few studies have been reported on the oxidation mechanism of this steel at high temperatures in air. It has been shown that 100 h of oxidation in air at 700 °C leads to the presence of $Cr_2O_3$ and $Fe_2O_3$ protuberant areas in the oxide scale [7]. Sobral et al. [8] showed that on injection moulding AISI 316L SS, the steel porosity not only increased the kinetics of the corrosion process, but also determined the nature of the resulting oxide layer with more iron oxides. It has been proposed that cerium and niobium additions lead to improved oxidation resistance of AISI 316L SS during oxidation at 700 °C in dry air [9]. Additions of yttria also lead to an increased oxidation resistance at 800 °C [10]. Other studies have shown that titanium coatings [11–14] or a laser-modified surface can be applied on AISI 316L SS materials to improve tribological properties [15, 16]. After oxidation at 900 °C, it is proposed that X-ray diffractograms indicate the presence of $NiFe_2O_4$, $Fe_2O_3$ and/or $(Fe_{0.6}Cr_{0.4})_2O_3$ [17]. Several studies proposed that, at high temperature, chromia forming alloys such as AISI 316L SS exhibit an oxide growth leading mainly to $Cr_2O_3$ and spinel-type oxide formation. However, the oxides actually present at 900 °C have never been identified. In situ X-ray diffraction studies can now be performed on AISI 316L SS specimens at 900 °C to analyse the oxides growing at this temperature. In the present work, this technique has been used to determine if a change in the structural composition of the layer occurs with time and if oxide phase transitions occur during cooling to room temperature, as has been demonstrated for AISI 304 SS [18]. This author also proposed that the formation of a protective $Cr_2O_3$ layer is favoured by the establishment of a continuous silica sublayer at the internal oxide–metal interface. Nevertheless, at 900 °C a breakaway oxidation behaviour was observed after about 40 h of oxidation. This phenomenon is related to the initial nucleation of $Fe_7SiO_{10}$, which traps silicon within the oxide scale and inhibits its segregation at the internal interface. Then, the high oxidation rate is due to the lack of a continuous silica layer at the internal interface,

H. Buscail (✉) · S. El Messki · F. Riffard · S. Perrier · R. Cueff · C. Issartel
LVEEM, Laboratoire Vellave sur l'Elaboration et l'Etude des Matériaux, EA 3864, Université de Clermont Ferrand, 8 rue J.B. Fabre, BP 219, LE PUY-en-VELAY 43006, France
e-mail: buscail@iut.u-clermont1.fr

which leads to the formation of less protective iron-containing oxides [19].

From the literature, the AISI 316L SS oxidation has been generally studied at temperatures lower than 900 °C and primarily between 300 and 700 °C. In this temperature range the oxide scale appears to consist of iron-containing oxides, which are not as protective as chromia scales. Therefore, it is of interest to test this steel to analyse the composition of scale formed in a relatively high temperature range where chromia is expected. The aim of the present work is to determine the oxidation mechanism of the AISI 316L SS at 900 °C and try to explain the good oxide scale adherence. The role of molybdenum on the AISI 316L SS oxidation process will be discussed with respect to the results obtained under the same conditions on the molybdenum free alloy AISI 304 SS.

## Experimental details

The materials used in the present work were an AISI 316L and an AISI 304 austenitic SS. The two SS compositions are given in Table 1. The specimens, provided by ArcelorMittal–Imphy, were polished on SiC paper up to the 800 polishing grade, then washed with ethanol and finally dried under a hot draught prior to isothermal oxidation at 900 °C.

The kinetic results obtained under isothermal conditions (90 h at 900 °C) in air were recorded using a Setaram TG-DTA 92-1600 microthermobalance. The *in situ* characterization of the oxide scales was carried out in a high temperature MRI chamber adapted on an X-ray Philips X' PERT MPD diffractometer (copper radiation, $\lambda k = 0.154$ nm). The morphology of the external interface as well as the cross sections was observed using a Scanning Electron Microscope (SEM). The analysis of the scale was performed using energy dispersive X-ray spectroscopy (EDS).

## Results

### Kinetics

The mass gain curve per unit area is given in Fig. 1. The thermogravimetric analysis was carried out for 90 h at 900 °C in air. For the AISI 304 specimens, the kinetic curve exhibited an initial parabolic regime ($kp = (2.0 \pm 0.2)\ 10^{-12}\ g^2\ cm^{-4}\ s^{-1}$) during the first 40 h of the oxidation test. This initial stage was followed by a breakaway oxidation regime leading to a significant mass gain after 90 h of exposure (2.3 mg $cm^{-2}$). For the AISI 316L SS specimens, a parabolic regime was observed throughout the 90 h oxidation test ($kp = (1.9 \pm 0.2)\ 10^{-13} g^2\ cm^{-4}\ s^{-1}$). The oxidation rate was slightly lower with AISI 316L specimens compared to the parabolic regime observed for the AISI 304 SS samples during the first 40 h at 900 °C.

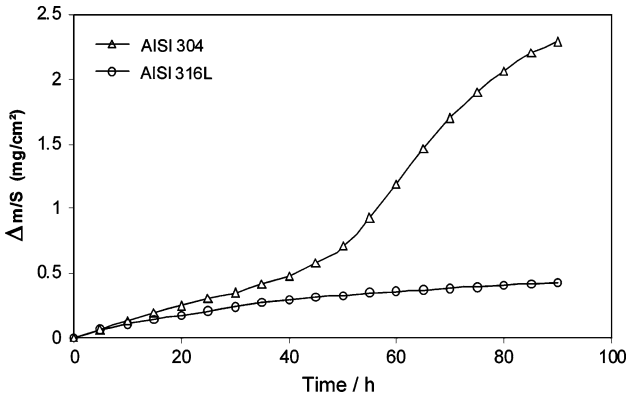


**Fig. 1** Mass gain curve obtained during isothermal oxidation of AISI 316L SS and AISI 304 SS in air at 900 °C

### Scale morphology

The morphology of the scale formed on AISI 316L SS oxidized during 90 h in air at 900 °C is presented in Fig. 2. No scale spallation was observed on the surface. This scale exhibited octahedral grains and plate-like grains. EDS

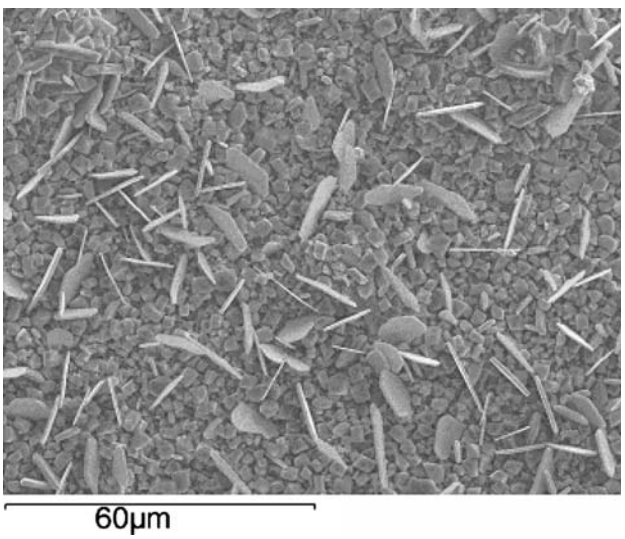


**Fig. 2** SEM micrograph showing the structure of the outer grains observed on the AISI 316L SS surface oxidized at 900 °C in air for 90 h

**Table 1** Composition of AISI 304 SS and AISI 316L SS (weight %)

| Alloy | Fe | Cr | Ni | Mo | Mn | Si | C |
|---|---|---|---|---|---|---|---|
| AISI 304 SS | Bal. | 17.9 | 9.05 | 0.15 | 1.52 | 0.47 | 0.053 |
| AISI 316L SS | Bal. | 17.7 | 10.9 | 2.16 | 1.57 | 0.55 | 0.023 |

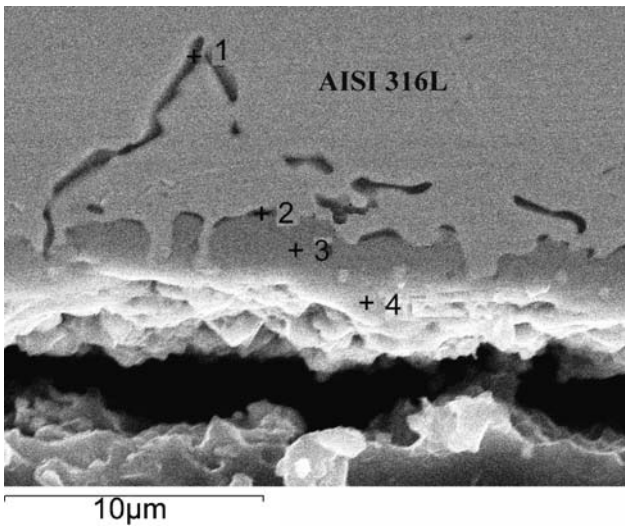


**Fig. 3** SEM cross-section on the AISI 316L SS oxidized at 900 °C in air for 90 h

analysis of the sample surface shows the presence of manganese, chromium and oxygen.

SEM examinations were carried out on the specimen cross section (Fig. 3) to estimate the scale thickness and to identify the elements constituting the oxide scale. After 90 h of oxidation at 900 °C, the adherent scale was about 3 µm thick and this scale exhibited internal oxidation along the alloy grain boundaries.

Figure 4 shows the EDS analyses performed on the cross section (Fig. 3). Manganese and chromium were located at the scale/air interface (spectrum 4). The middle part of the oxide scale was mainly composed of chromium oxide along with a small amount of iron and silicon (spectrum 3). EDS spectrum 1 shows that molybdenum is mainly located along the steel grain boundaries with silicon as oxide precipitates 10 µm deep inside the metallic matrix. EDS spectrum 2 exhibits that at the internal oxide–metal interface the amount of molybdenum appears to be important but silicon is not detected. It should be noticed that the oxide scale is thicker when molybdenum is detected at the internal interface.

### In situ X-ray diffraction results

The oxide scale formed on AISI 316L was analysed by in situ XRD on the metallic substrate at 900 °C, in air (Fig. 5). At 900 °C, it was noted that the dilatation of the metallic structure induces a shift of the diffraction peaks of AISI 316L to lower angle values. After cooling to room temperature, the AISI 316L SS peaks were again normally placed. No shift was observed on the oxides peak location due to the very low dilatation of oxides. Figure 5 shows the presence of $Mn_{1.5}Cr_{1.5}O_4$ (JCPDS 33-0892) and $Cr_2O_3$ (JCPDS 38-1479). It appears that both oxides nucleate simultaneously on the specimen surface during the first hour of oxidation and remain together at the external interface. No other oxides were formed during the 30 h oxidation test. According to the SEM cross-section observation obtained after 90 h of oxidation, it appears that $Mn_{1.5}Cr_{1.5}O_4$ is mainly located at the external interface and the $Cr_2O_3$ scale forms at the internal interface.

Figure 5 also shows that the in situ XRD patterns obtained after 30 h of oxidation is similar to the one obtained after cooling to room temperature. This indicates that no phase transition or scale spallation occurred during cooling. Finally, the in situ XRD results showed that no iron- or nickel-containing oxides were present on this substrate at 900 °C. Nevertheless, from Fig. 5, it appears that molybdenum-containing oxides could not be detected on the XRD patterns after 30 h of oxidation. In order to identify the molybdenum-containing oxides and better explain the role of this element, XRD was performed after a longer-term testing (90 h) (Fig. 6).

The XRD pattern in Fig. 6 shows that molybdenum was detected as $NiMoO_4$ (JCPDS 33-0948) after 90 h of oxidation at 900 °C. According to some authors, only one ternary phase, $NiMoO_4$, was found to exist in the system (NiO–$MoO_2$). The Gibbs energy of formation of $NiMoO_4$ from $NiO + MoO_2 + ½O_2 = NiMoO_4$ is $\Delta Gr° = -201{,}195 + 69.7\ T\ (\pm 400)\ J\ mol^{-1}$ [20]. SEM and EDS results have shown that this oxide was present at the internal interface and along the metallic grain boundaries (see Figs. 3 and 4). It was not detected after 30 h of oxidation owing to its low amount under the oxide scale at this oxidation stage.

## Discussion

Kinetic results have been obtained for AISI 316L SS between 800 and 1,000 °C. The parabolic behaviour was always followed in this temperature range. This permitted the calculation of the parabolic rate constants $k_p$ at each temperature (see Table 2).

The activation energy ($E_a$) was calculated from the slope of the Arrhenius plots of the $k_p$ values, $E_a = 220 \pm 30\ kJ\ mol^{-1}$. This value is close to the one generally encountered in the literature when $Cr_2O_3$ is formed on the alloys in this temperature range [21, 22]. This activation energy is in good agreement with the SEM cross section observation (Fig. 3) and in situ XRD (Fig. 5) showing that the scale was mainly composed of a continuous chromia scale, which acted as a diffusion barrier. Inside the scale, silica was not detected by XRD due to its amorphous state. Figure 6 shows that molybdenum was detected by XRD as $NiMoO_4$ (JCPDS 33-0948) after 90 h of oxidation at 900 °C. According to our results, the good kinetic

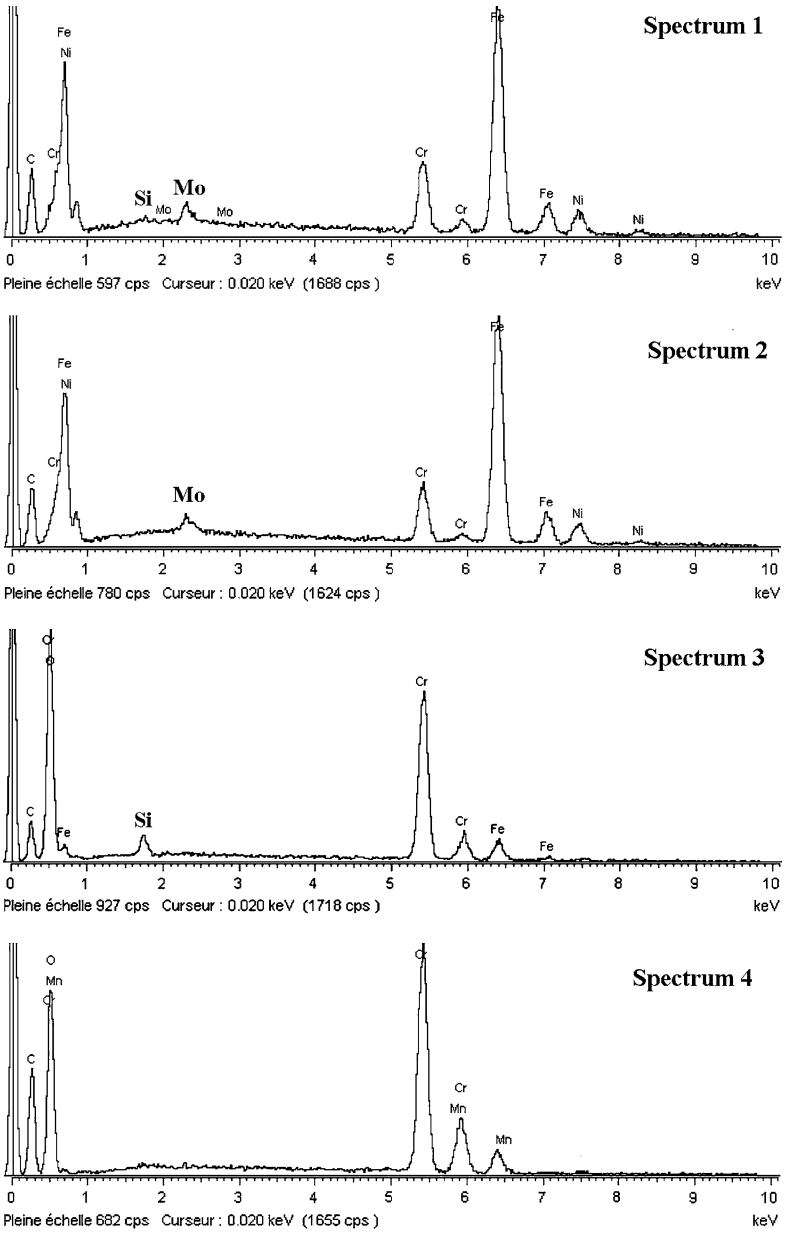


**Fig. 4** EDS spectra obtained on the cross section of AISI 316L SS oxidized at 900 °C in air for 90 h

behaviour appears to be mainly due to the absence of iron oxides in the scale (Fig. 5).

The scale surface and cross section micrographs (Figs. 2 and 3), also revealed that the oxide scale was adherent to steel substrate. Silicon and molybdenum have been found along the steel grain boundaries and molybdenum was detected alone at the metal/oxide interface (Fig. 4). We have also observed a keying effect between the scale and the metallic matrix due to the growth of internal oxide protrusions (Fig. 3). Our results obtained at 900 °C are in accordance with those of Sobral et al. [8], which studied the AISI 316L SS oxidation between 700 and 900 °C. These authors have also shown the presence of $(Mn_{1.5}Cr_{1.5})O_4$ and $Cr_2O_3$ after long exposure tests at 900 °C.

## Influence of silicon

For the AISI 304 SS specimens oxidized at 900 °C, Riffard et al. [19] have shown that after 90 h of oxidation, the scale was composed of a thick non-adherent oxide scale. In situ X-ray diffraction analyses have shown that the oxide scale formed on AISI 304 SS was composed of iron-containing oxides such as $FeCr_2O_4$, $Fe_2O_3$, $Fe_7SiO_{10}$ and $Mn_{1.5}Cr_{1.5}O_4$. These authors proposed that at 900 °C, the $Fe_7SiO_{10}$ phase was responsible for the relatively poor oxidation behaviour of AISI 304 SS by hindering the protective silica formation at the internal interface [19]. For the same oxidation temperature, the AISI 316L SS specimens showed a much better oxidation behaviour concerning the scale structure (no iron oxides) and

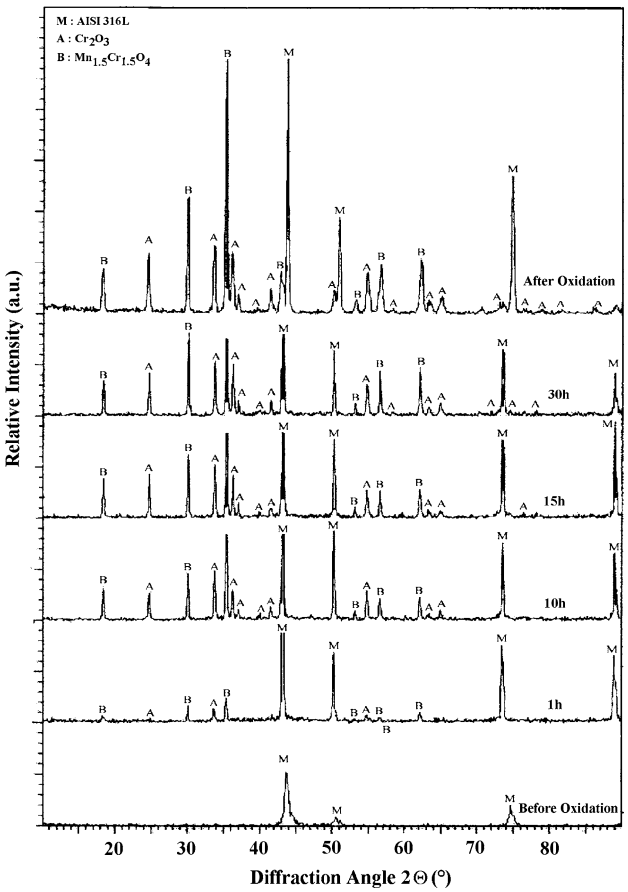


**Fig. 5** In situ XRD patterns obtained from the AISI 316L SS sample during isothermal oxidation at 900 °C in air

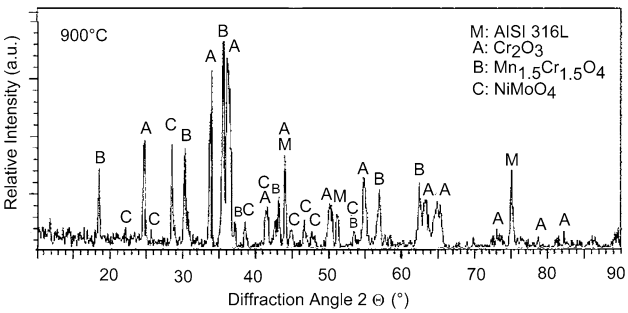


**Fig. 6** XRD performed on the AISI 316L SS sample after 90 h of isothermal oxidation at 900 °C in air

**Table 2** $k_p$ values obtained on AISI 316L SS between 800 and 1,000 °C

| Temperature | $k_p$ ($g^2$ $cm^{-4}$ $s^{-1}$) |
|---|---|
| 800 °C | $4.0 \pm 10^{-14}$ |
| 900 °C | $1.9 \pm 10^{-13}$ |
| 1,000 °C | $2.6 \pm 10^{-12}$ |

adherence (keying effect). The main difference between the oxidation behaviour of AISI 304 and AISI 316L steels appears to be related to the presence of increased levels of molybdenum in the AISI 316L SS specimens compared to the AISI 304 SS specimens. Molybdenum is generally added to the AISI 316L as a solid-solution strengthener. Nevertheless, with respect to the oxidation resistance, molybdenum can be undesirable because $MoO_3$ tends to volatilize or melt at high temperatures [7].

For chromia-forming alloys, the role of silicon as a protective element has been more extensively examined. Even though too high an amount of silicon is considered to be detrimental for the steel mechanical properties [23], its addition generally improves the steel oxidation resistance of the steel. Some authors [24–26] have stated that silicon segregates to the oxide/alloy interface and blocks the iron cationic diffusion. Silicon is then supposed to be present as a silica film, which lowers the oxidation rate of the steel. The high oxygen affinity of silicon permits its internal oxidation, developing $SiO_2$ precipitates along the alloy grain boundaries [27, 28]. Thus, silica acts as a diffusion barrier and leads to a keying effect of the chromia scale on the substrate [29, 30]. Silica will lower the porosity at the internal interface acting as vacancies sinks [31]. Silicon also reduces the amount of non-protective iron oxides inside the scale [32] and hinders the iron-rich nodule formation [25]. It has been shown by Paùl et al. that during the oxidation of a AISI 304-type SS between 900 and 1,000 °C, a maximum of 0.88 wt% silicon content led to the formation of a chromia scale. It should be noticed that the studied steel was manganese-free and that the comparison with manganese-containing steels is then not very easy [33]. On the other hand, it appears that too high an amount of silicon induced more scale spallation between the alloy and the silica scale or at the silica/chromia interface [26]. This is the reason why silicon is rarely added at levels of more than 1 wt%. One should also note that the presence of chromium is necessary to avoid the fayalite $Fe_2SiO_4$ formation, which is a very poor diffusion barrier [34, 35]. According to Stott et al. [35], the necessary amount of silicon needed to the $SiO_2$ formation can be lower when the chromium content increases.

## Role of molybdenum

Our results showed that at 900 °C, molybdenum was detected at the internal oxide–metal interface. The absence of Mo in the outer part of the scale may be the result of the volatility of surface $MoO_3$ oxides (Figs. 3 and 4). It should also be noticed that at 900 °C, the temperature seems to be sufficiently low to avoid the complete molybdenum volatilization from the steel surface [7] and permit the $NiMoO_4$

detection by XRD after 90 h of oxidation (Fig. 6). It can be envisaged that the $NiMoO_4$ formation at the internal interface does not need the previous formation of NiO and $MoO_2$ but can be the result of a direct combination of the elements under the low oxygen dissociation pressure under the $Cr_2O_3$ scale.

It has been proposed that a Mo–Si–O amorphous phase (not detectable by XRD) could form instead of $SiO_2$ and will show better protective properties [36]. At 900 °C, the effect of an amorphous phase cannot be envisaged at the oxide/steel interface because silicon has not been detected at this place. As observed on Fig. 3, the good scale adherence seems to be better related to a pegging effect at the internal interface. Then, internal oxidation leading to the pegging effect appears to be promoted by the presence of molybdenum detected by EDS at the internal interface (Figs. 3 and 4).

Even though they contain similar silicon contents, AISI 316L SS shows a relatively better behaviour compared with AISI 304 type steel at 900 °C; chromia scale adherence is improved and iron-containing oxides are not formed (Fig. 5). This is due to the 2 wt% molybdenum content of the AISI 316L SS. Other authors have shown that a limited amount of silicon can be added to the alloys. The addition of molybdenum permits addition of a higher content of protective element to the 0.5 wt% silicon generally introduced in such SSs. Then, 2 wt% molybdenum shows a quantitative effect on the AISI 316L SS oxidation protection without the over-doping effects encountered with the high silicon contents [26].

Moreover, spectrum 2 on Fig. 4 indicates that silicon is not present at the internal interface. Spectrum 3 on Fig. 4 shows that silicon and iron are present inside the scale. It could correspond to the formation of an iron silicate ($Fe_7SiO_{10}$) as was observed on AISI 304 SS specimens [19–21]. Nevertheless, our XRD results did not permit showing the presence of such an iron silicate inside the oxide scale formed on AISI 316L, probably due to its too low amount. Thus, it is proposed that the main effect of molybdenum at 900 °C is to replace silica at the internal interface. It then hinders the massive outward iron diffusion and the poor oxidation behaviour generally observed on molybdenum free alloys. The scale adherence is improved by a keying effect at the internal interface.

## Conclusion

In situ X-ray diffraction was used to identify the oxides formed on the AISI 316L SS during isothermal oxidation at 900 °C in air. Our results showed the presence of $Mn_{1.5}Cr_{1.5}O_4$ (JCPDS 33-0892) and $Cr_2O_3$ chromia (JCPDS 38-1479) growing simultaneously on the specimen surface. SEM cross-section observations revealed that the relatively high $Mn_{1.5}Cr_{1.5}O_4$ peak intensity was not due to a high proportion of this oxide in the scale but due to the location of this oxide at the external interface. No phase transitions or scale spallation was observed during cooling to room temperature. The XRD results showed that no iron oxides are formed on AISI 316L SS at 900 °C.

A comparison with the results obtained for AISI 304 SS enabled the role of molybdenum on the oxidation process of AISI 316L SS (containing 2 wt% Mo) to be examined. It was shown that molybdenum plays a protective role. Moreover, it is possible to add a high content of molybdenum in SS compared to the silicon level generally used. This high protective element content hindered the iron outward diffusion and led to the lower growth rate and better scale adherence. The good scale adherence was also related to a keying effect at the internal interface. At 900 °C, Mo was mainly located as a $NiMoO_4$ mixed oxide at the internal interface and along the steel grain boundaries. It is proposed that the main protective effect of molybdenum is to replace the missing silica scale at the internal interface during oxidation of this alloy at 900 °C.

## References


1. Johnson AL, Parsons D, Manzerova J, Perry DL, Koury D, Hosterman B et al (2004) J Nucl Mater 328:88. doi:10.1016/j.jnucmat.2004.03.006
2. Syed AA, Denoirjean TA, Fauchais P, Labbe JC (2006) Surf Coat Technol 20:4368. doi:10.1016/j.surfcoat.2005.02.156
3. Pitter J, Cerny F, Cizner J, Suchanek J, Tischler D (2005) Surf Coat Technol 200:73. doi:10.1016/j.surfcoat.2005.02.059
4. Kim S-G, Hong M-Z, Yoon SP, Han J, Nam SW, Lim TH et al (2003) J Sol–Gel Sci Technol 28:297. doi:10.1023/A:1027466113372
5. Indacochea JE, Smith JL, Litko KR, Karell EJ, Raraz AG (2001) Oxid Met 55:1. doi:10.1023/A:1010333407304
6. Vernault C, Mendez J (1999) Ann Chimie Sci Materiaux 24:351. doi:10.1016/S0151-9107(99)80074-9
7. Wang X, Wang LF, Zhu ML, Zhang JS, Lei MK (2006) Trans Nonferrous Met Soc China 16:s676. doi:10.1016/S1003-6326(06)60276-8
8. Sobral AVC, Hierro MP, Pérez FJ, Ristow W Jr, Franco CV (2000) Mater Corros 51:791. doi:10.1002/1521-4176(200011)51:11<791::AID-MACO791>3.0.CO;2-1
9. Samanta SK, Mitra SK, Pa TK (2006) Mater Sci Eng A 430:242. doi:10.1016/j.msea.2006.05.063
10. Bautista A, Velasco F, Abenojar J (2003) Corros Sci 45:1343. doi:10.1016/S0010-938X(02)00217-2
11. Siva Rama Krishna D, Sun Y (2005) Surf Coat Technol 198:447. doi:10.1016/j.surfcoat.2004.10.102
12. Siva Rama Krishna D, Sun Y (2005) Appl Surf Sci 252:1107. doi:10.1016/j.apsusc.2005.02.046
13. Furman P, Gluszek J, Masalski J (1997) J Mater Sci Lett 16:471. doi:10.1023/A:1018564326769
14. Vigen Karimi M, Sinha SK, Kothari DC, Khannab AK, Tyagic AK (2002) Surf Coat Technol 158–159:609. doi:10.1016/S0257-8972(02)00319-5

15. Singh R, Dahotre NB (2005) J Mater Sci 40:5619. doi:10.1007/s10853-005-1449-2
16. Stokes PSN, Stott FH, Wood GC (1989) Mater Sci Eng A 121:549
17. Bautista A, Velasco F, Campos M, Rabanal ME, Torralba JM (2003) Oxid Met 59:373. doi:10.1023/A:1023000329514
18. Karimi N, Riffard F, Rabaste F, Perrier S, Cueff R, Issartel C et al (2008) Appl Surf Sci 254:2292. doi:10.1016/j.apsusc.2007.09.018
19. Riffard F, Buscail H, Caudron E, Cueff R, Issartel C, El Messki S et al (2004) Mater Sci Forum 461–464:175
20. Jacob KT, Kale GM, Iyengar GNK (1987) J Mater Sci 22:4274. doi:10.1007/BF01132018
21. Jacob YP, Haanappel VAC, Stroosnijder MF, Buscail H, Fielitz P, Borchardt G (2002) Corros Sci 44:2027. doi:10.1016/S0010-938X(02)00022-7
22. Chen JH, Rogers PM, Little JA (1997) Oxid Met 47:381. doi:10.1007/BF02134783
23. Armand F, Davidson JH (1990) In: Lacombe P, Baroux B, Beranger G (eds) Les Editions de Physique
24. Huntz AM (1995) Mater Sci Eng A 201:211
25. Basu SN, Yurek GJ (1991) Oxid Met 36:281. doi:10.1007/BF00662967
26. Evans HE, Hilton DA, Holm RA, Webster SJ (1983) Oxid Met 19:1. doi:10.1007/BF00656225
27. Landkof M, Levy AV, Boone DH, Gray R, Yaniv E (1985) Corros Sci 41:344
28. Aguilar G, Larpin JP, Colson JC (1992) Mémoires et Etudes Scientifiques 89:447
29. Seal S, Bose SK, Roy SK (1994) Oxid Met 41:139. doi:10.1007/BF01196647
30. Durham RN, Gleeson B, Young DJ (1998) Oxid Met 50:139. doi:10.1023/A:1018880019395
31. Nagai H (1989) Mater Sci Forum 43:75
32. Pérez FJ, Cristobal MJ, Hierro MP, Pedraza F (1999) Surf Coat Technol 120–121:442. doi:10.1016/S0257-8972(99)00503-4
33. Paúl A, Elmrabet S, Alves LC, Da Silva MF, Soares JC, Odriozola JA (2001) NIM Phys Res B 181:394. doi:10.1016/S0168-583X(01)00358-5
34. Manning MI (1983) Gesell Metall 1:283
35. Stott FH, Wood GC, Stringer J (1995) Oxid Met 44:113. doi:10.1007/BF01046725
36. Yanagihara K, Przybylski K, Mauryama T (1997) Oxid Met 47:277. doi:0.1007/BF01668515